The niobium and tantalum concentration in the mantle constrains the composition of Earth's primordial magma ocean

Dongyang Huang, James Badro, Julien Siebert

The niobium and tantalum concentration in the mantle constrains the composition of Earth's primordial magma ocean

Dongyang Huang[a,1], James Badro[a], and Julien Siebert[a,b]

[a]Université de Paris, Institut de physique du globe de Paris, CNRS, F-75005 Paris, France; and [b]Institut Universitaire de France, 75005 Paris, France

Edited by Ho-kwang Mao, Center for High Pressure Science and Technology Advanced Research, Shanghai, China, and approved September 23, 2020 (received for review April 24, 2020)

The bulk silicate Earth (BSE), and all its sampleable reservoirs, have a subchondritic niobium-to-tantalum ratio (Nb/Ta). Because both elements are refractory, and Nb/Ta is fairly constant across chondrite groups, this can only be explained by a preferential sequestration of Nb relative to Ta in a hidden (unsampled) reservoir. Experiments have shown that Nb becomes more siderophile than Ta under very reducing conditions, leading the way for the accepted hypothesis that Earth's core could have stripped sufficient amounts of Nb during its formation to account for the subchondritic signature of the BSE. Consequently, this suggestion has been used as an argument that Earth accreted and differentiated, for most of its history, under very reducing conditions. Here, we present a series of metal–silicate partitioning experiments of Nb and Ta in a laser-heated diamond anvil cell, at pressure and temperature conditions directly comparable to those of core formation; we find that Nb is more siderophile than Ta under any conditions relevant to a deep magma ocean, confirming that BSE's missing Nb is in the core. However, multistage core formation modeling only allows for moderately reducing or oxidizing accretionary conditions, ruling out the need for very reducing conditions, which lead to an overdepletion of Nb from the mantle (and a low Nb/Ta ratio) that is incompatible with geochemical observations. Earth's primordial magma ocean cannot have contained less than 2% or more than 18% FeO since the onset of core formation.

core formation | Nb/Ta ratio | metal-silicate partitioning | high pressure

Niobium and tantalum are among those "geochemical twins" (e.g., Zr and Hf, Mo and W) located vertically adjacent to each other in the periodic table that share similar chemical properties during planetary differentiation. As both refractory and lithophile elements, Nb and Ta may be assumed to have condensed into planetary bodies in chondritic ratio (1) yet solely remained in the silicate portion of planets after core–mantle (metal–silicate) differentiation. However, in contrast to other trace element ratios (e.g., Zr/Hf and Ce/Pb), which indicate the complementarity between Earth's mantle and (continental or oceanic) crust with respect to chondritic meteorites, Nb/Ta ratios in all major reservoirs of silicate Earth (the crust, depleted mid-ocean ridge basalt mantle, and ocean island basalts) are invariably subchondritic (<19.9) (2). This apparent deficit of Nb relative to Ta in the bulk silicate Earth (BSE), known as the "Nb paradox," has been attributed to 1) a hitherto unsampled reservoir with a superchondritic Nb/Ta ratio in the lowermost mantle formed by an ancient subducted crust as early as the Hadean (3–5) and/or 2) the sequestration of Nb into the core during core–mantle differentiation (6–8).

The metal–silicate partitioning behavior of Nb, a lithophile element, was first found to mimic that of V, a slightly siderophile element, at elevated pressures (25 GPa) (6).This invariably leads to an increase in Nb solubility in metal relative to Ta in a deep magma ocean and has been proposed as a reason for the subchondritic Nb/Ta ratio observed in the BSE. This requires, however, just as in the case of V, the magma ocean to start and remain very reducing (very low FeO concentration) for an extended period during core segregation. Reducing conditions were considered as the only pathway to an increase in the siderophility of V and Nb. Indeed, all experiments to date (performed in piston-cylinder or multianvil press up to ∼25 GPa) show that oxygen fugacity is the dominant parameter (that superimposes pressure [P], temperature [T], and composition) to incorporate Nb in the metal during core–mantle equilibration (7, 8), despite the dependence of partitioning on pressure and temperature (9–12). Further experiments, along with multistage core formation models confirmed that in order to match the Nb abundance and the Nb/Ta in the mantle by core formation alone, a highly reducing magma ocean (very low FeO concentration) was required, with a silicate liquid containing significantly less than 1 wt % FeO (7, 13, 14). The natural consequence of those findings was that the behavior of V and Nb (and to a lesser extent Cr and Ta) during core formation requires Earth to have accreted and remained very reduced for a significant amount of time.

The initiation of metal–silicate partitioning experiments in the laser-heated diamond anvil cell (LHDAC) extended the P and T conditions of metal–silicate experiments to those directly relevant (43 to 75 GPa and 3,000 to 4,400 K) to core formation on Earth (15). One of the new outcomes of this class of experiments was the significant increase in oxygen concentration in the metal

Significance

Silicate Earth is widely considered identical to chondrites in its refractory lithophile element ratios. However, its subchondritic Nb/Ta signature deviates from the chondritic paradigm. To resolve this Nb deficit, its sequestration in Earth's core under very reducing core-forming conditions has been proposed based on low-pressure data. Here, we show that under conditions relevant to core formation Nb is siderophile at high pressures under all redox conditions, corroborating Nb inventory in Earth's core. Further core formation modeling shows that Earth's core could have formed under moderately reducing or oxidizing conditions, whereas highly reducing conditions mismatch the geochemical observables; although Earth may have sampled a variety of reservoirs, it is problematic to accrete primarily from materials as reduced as enstatite chondrites.

Author contributions: J.B. and J.S. designed research; D.H. and J.B. performed research; D.H., J.B., and J.S. analyzed data; and D.H., J.B., and J.S. wrote the paper.

The authors declare no competing interest.

This article is a PNAS Direct Submission.

[1]To whom correspondence may be addressed. Email: huang@ipgp.fr.

This article contains supporting information online at https://www.pnas.org/lookup/suppl/doi:10.1073/pnas.2007982117/-/DCSupplemental.

at those conditions (16, 17) and its effect on the metal–silicate partitioning of trace elements. Other elements present in the metal (Si, S, and C) also affect metal–silicate partitioning, but their influences have been modeled and constrained extensively in the metallurgy literature (room pressure) and by large-volume (piston-cylinder and multianvil press) experiments at elevated pressure. Oxygen, on the other hand, requires extreme conditions of P–T to dissolve in the metal in sufficiently large amounts, and hence the effect of oxygen on trace-element metal–silicate partitioning was only recently quantified. The magnitude of those interactions with oxygen can be so dramatic in the final stages of core formation (highest P and T conditions) that the partitioning of siderophile (17, 18) and even nominally lithophile elements (19–22) is strongly affected. The magnitude of those effects is beyond merely quantitative and brings qualitative changes. Ref. 18 found that Cr and V become exceedingly siderophile at extreme P and T conditions, an effect largely due to the oxygen content of the metal. This provides a new pathway toward the sequestration of those elements in the core. To the traditional method of increasing their siderophility by partitioning under reducing conditions comes a new mechanism accomplishing the same by increasing the oxygen content of the core. Intriguingly, high oxygen contents in the core are indicative of rather oxidizing conditions, quite opposite to the classical pathway. Based on those two elements, ref. 18 relaxed the need for highly reducing conditions during prolonged periods of core formation on the basis of V and Cr partitioning.

The question now is whether the same holds for Nb and Ta, which are the remaining elements requiring such extremely reducing conditions during accretion and core formation, that is, whether increasing oxygen content of core-forming metal enhances the siderophile character of those two elements in a way that is compatible with the geochemical records (absolute concentrations and Nb/Ta in the mantle). We performed a series of metal–silicate partitioning experiments up to 94 GPa and 4,500 K in LHDACs and observed that both Nb and Ta also become more siderophile by interacting with oxygen dissolved in the liquid metal. Thermodynamic modeling of the global partitioning dataset (previous experiments augmented by our data) allowed us to unravel exceedingly large interaction parameters of Nb and Ta with oxygen in liquid iron, even larger than the ones found for Cr or V, and on the order of those found for U. Incorporating these into a multistage core formation model shows interestingly that highly reducing conditions, such as those posited in the literature fail to reproduce both the abundance of Nb and the Nb/Ta ratio in Earth's mantle (both are too low). Highly oxidizing conditions can satisfy the abundance of Nb but not the Nb/Ta ratio, which becomes too high. Only starting magma ocean compositions between 2 and 18 mol % FeO can satisfy the observables.

Results

Five superliquidus experiments were performed at various P–T conditions (*SI Appendix*, Table S1) in LHDACs. The starting metal, an Fe–Ni–V–Cr alloy, was synthesized in a 150-ton end-loaded piston cylinder press (*Materials and Methods*), whereas the starting silicates were glasses synthesized in a gas-mixing aerodynamic levitation laser furnace; starting compositions (analyzed by electron microprobe) are given in *SI Appendix*, Table S2. Similar to previous superliquidus metal–silicate partitioning experiments performed in DACs (16, 17, 19, 20, 23), quench texture was found in all of our experiments. As shown by a backscattered scanning electron microscopy (SEM) image in Fig. 1, the typical morphology that the sample inherited from quenching is a spherical metallic blob (bright sphere) embedded in a molten silicate (gray area), which is separated by a layer of untransformed solid glass from the diamond anvils. The unique texture was formed by the rapid exsolutions of Si–O-rich and Fe–Ni-rich phases (<200 nm) in the metal and silicate during quenching, respectively. Large window (raster-scanned electron beam) analysis shows chemical homogeneity in both phases over the entire recovered sample. The chemical composition measured by electron probe microanalyzer (EPMA) is reported in *SI Appendix*, Table S3.

The partitioning of Nb and Ta between metal and silicate occurs via an exchange reaction:

$$MO_{\frac{n}{2}} + \frac{n}{2}Fe = \frac{n}{2}FeO + M, \qquad [1]$$

where n is the valence of the cation M (Nb and Ta are both 5+) in the silicate melt. The metal–silicate partition coefficient of element M is $D_M = x_M/x_{MOn/2}$, where x the molar fraction. The exchange coefficient, $K_D(M) = D_M/D_{Fe}^{n/2}$, is a more suitable parameter to handle thermodynamically, because it conveniently removes the explicit dependence of partitioning on oxygen fugacity expressed by D_{Fe}, but more importantly because it is closely linked to the essential thermodynamic quantity governing reaction **1**, the equilibrium constant $K(M)$. The equilibrium constant $K(M)$ of reaction **1** can be explicitly rewritten in terms of exchange coefficient (K_D) and activity coefficients (γ) in the silicate and metallic phases and expressed as a function of P, T, and silicate melt composition by

$$\begin{aligned} logK(M) &= logK_D(M) + log\frac{\gamma_M^{metal}}{\left(\gamma_{Fe}^{metal}\right)^{\frac{n}{2}}} + log\frac{\left(\gamma_{FeO}^{silicate}\right)^{\frac{n}{2}}}{\gamma_{MO_{\frac{n}{2}}}^{silicate}} \\ &= a + \frac{b}{T} + \frac{c\cdot P}{T} + d\cdot\left(\frac{nbo}{t} - 2.7\right) \end{aligned}, \qquad [2]$$

where a is the entropy, b the enthalpy, and c the volume change of reaction **1**. Following previous studies of the valence of Nb and Ta in silicate melts (7, 11, 12, 24), we fixed the valence of Nb and Ta to pentavalent (5+; *SI Appendix*). The activity coefficient ratio in silicate (third term in Eq. **2**) for high-valence cations may vary largely and is hard to be evaluated due to the unavailability of relevant data. To account for the compositional effect of silicate melt on partitioning of highly charged cations, we introduced an empirical parameter *nbo/t* (25), the molar ratio of nonbridging oxygens (*nbo*) per tetrahedrally coordinated cations (t), which is an empirical proxy valid at low pressures where

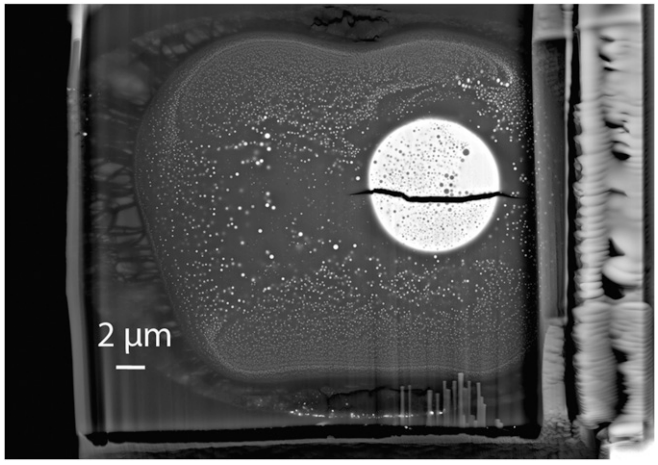

Fig. 1. Backscattered electron field emission SEM image of a focused ion beam section recovered from a superliquidus metal–silicate equilibration at 47 GPa and 4,100 K in the LHDAC. The quench morphology consists of a metallic blob (bright sphere) embedded in the silicate melt.

silicon is tetrahedrally coordinated. The *nbo/t* expresses the degree of polymerization of a silicate melt and was corrected to a value of 2.7 corresponding to the *nbo/t* of a pyrolitic melt (the correction was not used in all LHDAC data above 25 GPa; details are given in *SI Appendix*). Since the activity coefficients in the metal can be significantly influenced by light components (e.g., Si, O, S, and C) dissolved in liquid iron (26–29), we followed the interaction parameter approach (*SI Appendix*) to calculate the activity coefficients γ_{Fe} and γ_i (30). The calculated equilibrium constant K using the interaction parameter model was fitted to the thermodynamic model described in Eq. **2**, using multivariate least-squares linear regression (reported in Table 1). Previously published metal–silicate partitioning experiments with samples containing Nb (6, 7, 9, 11, 12, 16, 18, 31) or Ta (6, 7, 9–12) are compiled in Dataset S1; these data are plotted in Fig. 2, along with our data. It is noticeable that the present work fills in the gap of partitioning data for both Nb and Ta at the conditions of core formation (15).

P–T Dependence. The expanded P–T conditions obtained in LHDAC experiments allow for better constraints on the thermodynamic conditions during core–mantle (metal–silicate) differentiation. As shown in Table 1, the pressure effect (parameter c) on the partitioning of Nb is found to be negative, that is, Nb becomes less siderophile with increasing pressure, which is consistent with previous low-pressure results (9–12) but to a lesser magnitude, while for the partitioning of Ta the influence of pressure is statistically negligible, as evidenced by the P value of 0.8 (return to the null hypothesis) when incorporating the pressure term in the multivariate regression.

For both Nb and Ta, temperature increases their affinity for metallic phase (b is negative). The dependence of log K on temperature for Nb and Ta agrees with piston-cylinder and multianvil data (9–12) but is in contrast to ref. 7, who found negligible pressure and temperature effect. Because log K has a multivariate dependency on P, T, and *nbo/t*, and in order to compare things that are comparable, we corrected the dataset to zero pressure and pyrolitic silicate composition (*nbo/t* = 2.7) and plotted log K as a function of reciprocal temperature in Fig. 2. Plotting partitioning as a function of temperature is the classical way of presenting the data, but for the sake of completeness we also reported the same analysis as a function of *nbo/t* (by correcting to zero pressure and temperature; *SI Appendix*, Fig. S2) and as a function of P (by correction to zero temperature and pyrolitic composition with *nbo/t* = 2.7; *SI Appendix*, Fig. S3).

Metal Composition Dependence. While the starting metal contained neither oxygen nor any lithophile elements (*SI Appendix*, Table S2), oxygen, magnesium, and aluminum were observed along with siderophile elements in the recovered metal (*SI Appendix*, Table S3). The increasing solubility of these elements, especially oxygen, is intrinsically a temperature effect (16, 19). Light elements (e.g., C, S, Si, and O) dissolved in the liquid iron

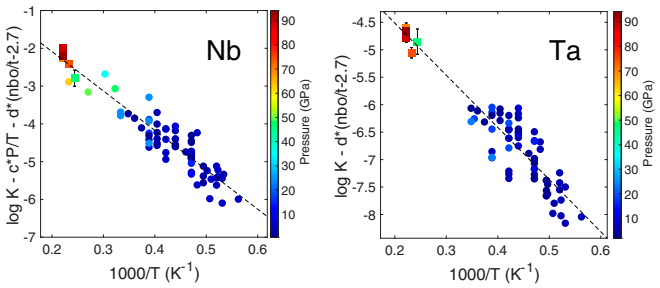

Fig. 2. Equilibrium constants (log K) for Nb and Ta as a function of reciprocal temperature (1,000/T). The dashed lines correspond to least-squares linear regressions to the data, and error bars (only for the data from this study, shown where larger than symbols) were propagated from the analytical uncertainties in *SI Appendix*, Table S3. Pressure is reported in symbol color. Experimental data for Nb are taken from refs. 6, 7, 9, 11, 12, 16, 18, and 31 (circles) and this study (squares). Ta data are taken from refs. 6, 7, and 9–12 (circles) and this study (squares). As shown in the *y*-axis legend, we are plotting equilibrium constants adjusted to zero pressure and pyrolitic silicate melt compositions, in order to compare things that are comparable.

are known to deviate the iron alloys from an ideal solution regarding metal–silicate partitioning. Using the activity model described in *SI Appendix*, we have modeled the effect of metal composition by fitting the interaction parameters, a constant that describes the interactions among solutes. In Table 1, the fitted absolute values of interaction parameter ε_i^O for Nb and Ta are much larger than those of ε_i^{Si}, ε_i^S, and ε_i^C, which means that oxygen dissolved in liquid iron has more pronounced influence on the partitioning of Nb and Ta than silicon, sulfur, or carbon does. As a result of their interactions with oxygen, Nb and Ta become more siderophile, though to different extents (the interaction parameter ε_{Ta}^O is almost twice that of ε_{Nb}^O).

Implication for Core Formation Modeling. The thermodynamic models of Nb and Ta metal–silicate partitioning used in recent models were derived from experiments performed at low to moderate pressures (<25 GPa), significantly lower than the putative conditions of core formation on Earth (40 to 75 GPa). As previously indicated, those thermodynamic models only allow a single pathway for Nb incorporation in the core, that of highly reducing initial conditions that were sustained for an extended period of time, to explain the subchondritic Nb/Ta ratio in the mantle. This has given new impetus for core formation occurring under very reducing conditions (7, 14). Here, our all-encompassing thermodynamic model (based on the previous data augmented by the high-pressure data obtained by LHDAC experiments) offers a second pathway for accomplishing the same requirement—that of oxygen incorporation in the metal.

We ran a campaign of multistage core formation models (15) using the thermodynamic parameters in Table 1. We started with

Table 1. Thermodynamic parameters of the metal–silicate partitioning of Nb and Ta

Element (i)	a	b, K	c, K/GPa	d	ε_i^O	ε_i^{Si}	ε_i^C	ε_i^S	ε_i^j	$\ln\gamma_i^0$	N	R^2
Nb	**0**	**−10,314 (108)**	**−67 (7)**	**−0.39 (4)**	**−34.9**	**−6.1**	**−5.2**	**0**	−0.7	−1.61	74	0.852
Ta	**−2.71 (26)**	**−9,270 (607)**	**0**	**−0.18 (5)**	**−60.6**	**−8.7**	**−10.5**	**0**	79.7	−3.22	72	0.906
O						−5			−1			
Si									12.4			

Parameters of Eq. **2** for Nb and Ta partitioning: a, b, and c represent the entropy, enthalpy, and volume change of reaction **1**; values in parentheses are SEs (1σ) obtained from the least-squares regressions. ε_i^j is the interaction parameter of element j on element i and γ_i^0 the activity coefficient of solute i at infinite dilution in liquid iron; interaction parameters in boldface are calculated from this study and other values are taken from metallurgy data (41). Interaction parameters and activity coefficients are reported at 1,873 K (details are given in *SI Appendix*). N is the number of data used in each thermodynamic modeling and R^2 the coefficient of determination of the fitted model.

different initial FeO concentrations in the magma ocean (ranging from 1 to 18 mol %) and allowed them to evolve linearly throughout accretion to reach the present-day value of 6 mol % at the end of accretion. Accordingly, the fO_2 is a free parameter in our models; however, the more reducing conditions follow closely the evolution of fO_2 proposed by ref. 14. We also tested two models proposed by refs. 7 and 10, where the initial FeO content is extremely low and the evolution of magma ocean FeO is sublinear (Fig. 3*A*). For each one of those magma ocean compositional models, we ran 136 multistage core formation models where the final depth of the magma ocean varied from 0 to 135 GPa (with 1-GPa increments); because we also tracked Ni and Co metal–silicate partitioning at the same time, we discriminated a range of pressures providing "valid" models, that is, those where their abundances matched the terrestrial mantle values.

For each compositional model, we therefore obtained a range of Nb and Ta concentrations in the mantle (corresponding to each model's valid range of final magma ocean pressures; *SI Appendix*, Fig. S4), which are reported in Fig. 3. The bulk core–mantle partition coefficient of Nb and Ta, as well as the Nb/Ta ratio in the BSE by the time Earth's core was formed, were plotted (Fig. 3) as a function of initial FeO content in the magma ocean. It is clear from this that Nb and Ta are more siderophile as the starting conditions are reducing (low FeO), evidenced by the high *Ds* in Fig. 3 *C* and *D*. On the other hand, the Nb/Ta ratio in the magma ocean rises with increasing initial FeO (Fig. 3*B*). Very reducing conditions prevailing for a long time (7, 10) end up with too high a D_{Nb}, or too low an Nb concentration in the mantle and a Nb/Ta ratio that is too subchondritic, lower than the overserved value. On the other end of the compositional range, a very oxidized magma ocean (18 mol % initial FeO) could match the mantle abundance of Nb but ends up with a subchondritic Nb/Ta ratio in the mantle which is too high compared to the observed value. The only magma ocean compositional models that satisfy both constraints, the Nb abundance in the mantle and its Nb/Ta ratio, are those where the initial FeO concentration is between 2 and 18 mol %. Interestingly, this range is in impeccable agreement with core formation models where the Si isotopic composition of the mantle was used as a constraint (32). We therefore conclude that neither extremely reducing nor highly oxidizing conditions can account for Earth's subchondritic Nb/Ta signature and Nb inventory. The magma ocean may still have started more reduced or more oxidized than the present-day mantle (and evolved toward it), but any extremes have to be ruled out.

In order to quantify the extent of oxygen interaction on the outcome of core formation models, we ran the same series of models, setting the oxygen interaction parameters to 0. Doing this, the sole difference is that the effect oxygen dissolved in the core stops acting on Nb and Ta partitioning. The results are plotted in *SI Appendix*, Fig. S5, following the same rationale of Fig. 3. We observed a less protracted solution space, biased toward reducing conditions. The affinity for liquid iron decreases for both Nb and Ta, though to different degrees, which propels

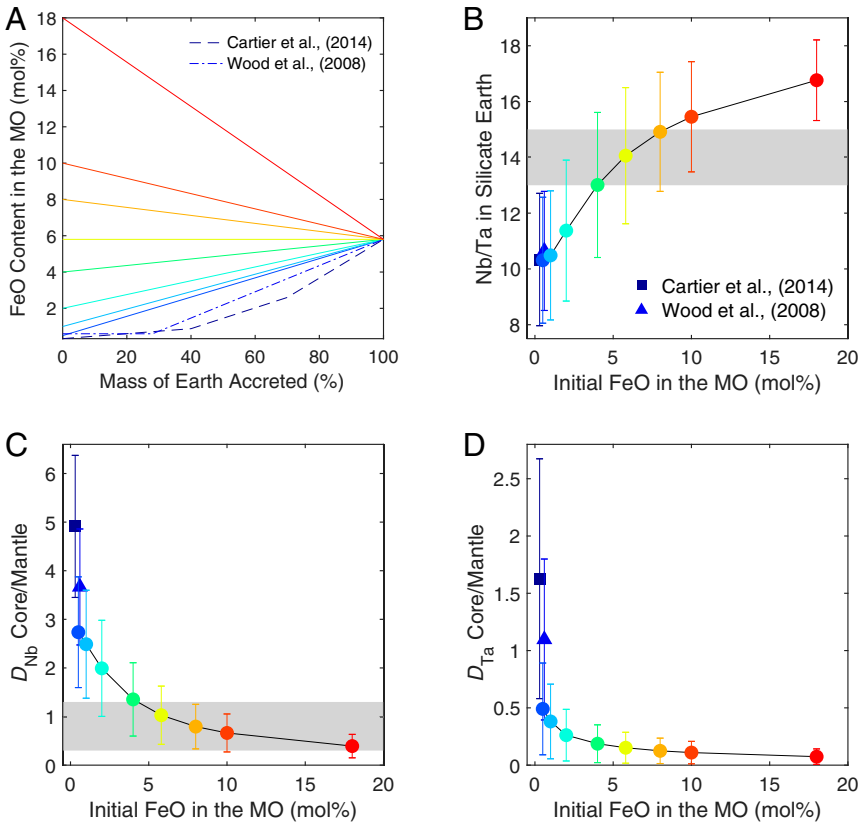

Fig. 3. (*A*) The evolution of FeO content in the magma ocean (MO) during Earth's accretion. The color is coded according to redox states of the MO, with warmer colors corresponding to more oxidizing conditions. (*B*) Nb/Ta ratio in the BSE, and core–mantle partition coefficients of Nb (*C*) and Ta (*D*) at the end of Earth's accretion, as a function of initial FeO content in the magma ocean. Each point in *B–D* corresponds to an output of the multistage core formation model with a linear evolution of fO_2 in *A*, except for the squares and triangles that follow the fO_2 paths proposed by refs. 7 and 10, dashed and dashed-dotted lines in *A*, respectively. The uncertainties are the intervals of *y* in the pressure range (40 to 70 GPa) of the MO allowed by the observables of Ni and Co partitioning (*SI Appendix*). The horizontal bars correspond to the targets, that is, present-day bulk *D* between core and mantle or subchondritic Nb/Ta ratio in the BSE. The observed subchondritic Nb/Ta ratio and Nb abundance in the BSE are matched with the initial FeO concentration from 2 to 18%.

their ratio upward and shifts the solution to more reducing conditions. It highlights that oxidizing conditions, with their associated oxygen enrichment of the cores, increase the siderophile behavior of both Nb and Ta, which allows for a much larger range of magma ocean compositions to match the relevant geochemical observables. This gracefully explains why previous core formation scenarios found solutions only through initially reduced conditions (7, 10, 14, 31), and why the actual solution space is broader now and encompasses a wider range of redox conditions going all of the way into "oxidizing" models.

The other alternatives for the Nb depletion in the BSE include 1) volatile loss of Nb during incomplete accretion and 2) a "hidden" reservoir with superchondritic Nb/Ta ratio in the lower mantle. The first assumption is not supported by the calculated condensation temperatures for Nb and Ta (33). As there is no direct evidence for a large-scale superchondritic Nb/Ta reservoir in Earth (3–5), heat flux data seem to argue against an early-formed hidden layer enriched in incompatible elements (34). Our data and the models it reveals show that the niobium deficit in Earth's mantle and its subchondritic Nb/Ta ratio can be explained by core formation alone. This can take place in an initial magma ocean with composition bracketing that of enstatite and carbonaceous/ordinary chondrites, that is, moderately reducing or oxidizing conditions, without the ad hoc hidden reservoir. It does exclude, however, the most extreme conditions that have been deemed most plausible until now.

Materials and Methods

Starting Materials. The silicate starting materials were synthesized using levitation method according to a pyrolitic composition (35) without FeO. The metallic starting materials were either commercial reagent Fe-rich metal balls (91% Fe + 9% Si) or trace-element-bearing iron–nickel alloy synthesized in a piston-cylinder apparatus at Institut de Physique du Globe de Paris (IPGP) (details for sample synthesis can be found in *SI Appendix*). Starting materials were analyzed by an EPMA at Camparis to confirm the chemical homogeneity (*SI Appendix*, Table S2). The silicate glasses were polished down to ∼20 μm thick and subsequently machined into small disks suitable for DAC loading. Synthesized metal was recovered and finely ground to serve as starting metal for DAC experiments. In order to test their lithophility, that is, the direction of the partitioning, all of the interested metals (Nb and Ta) were added in the starting silicates (*SI Appendix*, Table S2).

LHDAC Experiments. Symmetric DACs were used to generate high pressure. Diamond anvils with flat culet diameters of 200 μm or 300 μm were used. Re gaskets were preindented to 40 to 50 μm thick with a gasket hole of ∼100 μm or 150 μm in diameter to serve as a sample chamber. The silicate glasses were double-polished to 18 to 23 μm and cut into disks adapted to the diameter (10 μm smaller) of the sample chamber (gasket hole), using a picosecond laser micromachining instrument. The disks were loaded directly on both diamond culets, and a single chunk of metal was loaded in the center of one of the disks; once closed, the sample consists of a silicate capsule with the metal sitting in its middle (both radially and axially). The silicate disks also served as thermal and chemical insulator during laser heating.

Sample assembly was compressed to target pressures and subsequently heated from both sides using a fiber laser (λ = 1,070 nm, 200 W) with a focused beam size of ∼20 μm in diameter. Typical heating lasted up to several minutes, with temperature ramping at first and then held at maximal (target) temperature for at least 60 s before instantaneous (a few 10s of microseconds) quench. Time series experiments under similar extreme conditions have demonstrated the achievement of equilibrium in a few seconds (9, 36). To make sure the pyrolite fully melted, all runs were conducted well above the liquidus of pyrolite (e.g., 4,500 K at 94 GPa) (37, 38). Temperature was measured every second (simultaneously from both sides) by fitting the visible portion of the black-body radiation (500 to 750 nm) of the hot spot with an uncertainty around ±250 K (39). Pressure was determined by diamond Raman spectroscopy of the anvils before heating (40) and corrected for thermal pressure following $\Delta P = 2.7$ MPa/K (16, 37, 38). Samples were recovered from the laser-heated areas (Fig. 1) using a focused ion beam instrument (Zeiss Auriga 40 at IPGP) and analyzed by an EPMA (Cameca SX-five) at Camparis. Details of sample recovery and chemical analysis are described in *SI Appendix*.

Data Availability. All study data are included in the paper, *SI Appendix*, and Datasets S1 and S2.

ACKNOWLEDGMENTS. We thank Nicolas Wehr for help in high-pressure experiments; Stephan Borensztajn for assistance with focused ion beam samples preparation, electron microscopy and microanalysis; and Frederic Moynier and Hugh St.C. O'Neill for discussions. We also thank three anonymous reviewers for their constructive comments and the editor for handling this manuscript. The research leading to these results has received funding from the European Research Council under the European Community's Seventh Framework Programme (FP7/2007-2013) / ERC Grant 207467. We acknowledge the financial support of the UnivEarthS Labex program at Sorbonne Paris Cité (ANR-10-LABX-0023 and ANR-11-IDEX-0005-02). J.S. and D.H. acknowledge support from the French National Research Agency (ANR project VolTerre, Grant ANR-14-CE33-0017-01). Parts of this work were supported by IPGP multidisciplinary program PARI (Plateforme d'analyse haute résolution), and by Paris–IdF region SESAME (Soutien aux Equipes Scientifiques pour l'Acquisition de Moyens Expérimentaux) Grant 12015908.

1. H. Palme, H. S. C. O'Neill, "Cosmochemical estimates of mantle composition" in *Treatise on Geochemistry: Second Edition*, (Elsevier Ltd., 2014), Vol. 3, pp. 1–39.
2. C. Münker *et al.*, Evolution of planetary cores and the Earth-Moon system from Nb/Ta systematics. *Science* **301**, 84–87 (2003).
3. R. L. Rudnick, M. Barth, I. Horn, W. F. McDonough, Rutile-bearing refractory eclogites: Missing link between continents and depleted mantle. *Science* **287**, 278–281 (2000).
4. B. S. Kamber, K. D. Collerson, Role of 'hidden' deeply subducted slabs in mantle depletion. *Chem. Geol.* **166**, 241–254 (2000).
5. O. Nebel, W. Van Westrenen, P. Z. Vroon, M. Wille, M. M. Raith, Deep mantle storage of the Earth's missing niobium in late-stage residual melts from a magma ocean. *Geochim. Cosmochim. Acta* **74**, 4392–4404 (2010).
6. J. Wade, B. J. Wood, The Earth's 'missing' niobium may be in the core. *Nature* **409**, 75–78 (2001).
7. C. Cartier, T. Hammouda, M. Boyet, M. A. Bouhifd, Redox control of the fractionation of niobium and tantalum during planetary accretion and core formation. *Nat. Geosci.* **7**, 573–576 (2014).
8. C. Munker, R. O. C. Fonseca, T. Schulz, Silicate Earth's missing niobium may have been sequestered into asteroidal cores. *Nat. Geosci.* **10**, 822–826 (2017).
9. A. Corgne, S. Keshav, B. J. Wood, W. F. McDonough, Y. Fei, Metal-silicate partitioning and constraints on core composition and oxygen fugacity during Earth accretion. *Geochim. Cosmochim. Acta* **72**, 574–589 (2008).
10. B. J. Wood, J. Wade, M. R. Kilburn, Core formation and the oxidation state of the Earth: Additional constraints from Nb, V and Cr partitioning. *Geochim. Cosmochim. Acta* **72**, 1415–1426 (2008).
11. U. Mann, D. J. Frost, D. C. Rubie, Evidence for high-pressure core-mantle differentiation from the metal-silicate partitioning of lithophile and weakly-siderophile elements. *Geochim. Cosmochim. Acta* **73**, 7360–7386 (2009).
12. J. Siebert, A. Corgne, F. J. Ryerson, Systematics of metal-silicate partitioning for many siderophile elements applied to Earth's core formation. *Geochim. Cosmochim. Acta* **75**, 1451–1489 (2011).
13. D. C. Rubie *et al.*, Heterogeneous accretion, composition and core–mantle differentiation of the Earth. *Earth Planet. Sci. Lett.* **301**, 31–42 (2011).
14. D. C. Rubie *et al.*, Accretion and differentiation of the terrestrial planets with implications for the compositions of early-formed Solar System bodies and accretion of water. *Icarus* **248**, 89–108 (2015).
15. J. Badro, J. P. Brodholt, H. Piet, J. Siebert, F. J. Ryerson, Core formation and core composition from coupled geochemical and geophysical constraints. *Proc. Natl. Acad. Sci. U.S.A.* **112**, 12310–12314 (2015).
16. J. Siebert, J. Badro, D. Antonangeli, F. J. Ryerson, Metal-silicate partitioning of Ni and Co in a deep magma ocean. *Earth Planet. Sci. Lett.* **321–322**, 189–197 (2012).
17. R. A. Fischer *et al.*, High pressure metal-silicate partitioning of Ni, Co, V, Cr, Si, and O. *Geochim. Cosmochim. Acta* **167**, 177–194 (2015).
18. J. Siebert, J. Badro, D. Antonangeli, F. J. Ryerson, Terrestrial accretion under oxidizing conditions. *Science* **339**, 1194–1197 (2013).
19. J. Badro, J. Siebert, F. Nimmo, An early geodynamo driven by exsolution of mantle components from Earth's core. *Nature* **536**, 326–328 (2016).
20. I. Blanchard, J. Siebert, S. Borensztajn, J. Badro, The solubility of heat-producing elements in Earth's core. *Geochem. Perspect. Lett.* **5**, 1–5 (2017).
21. B. A. Chidester, Z. Rahman, K. Righter, A. J. Campbell, Metal-silicate partitioning of U: Implications for the heat budget of the core and evidence for reduced U in the mantle. *Geochim. Cosmochim. Acta* **199**, 1–12 (2017).
22. J. Badro *et al.*, Magnesium partitioning between Earth's mantle and core and its potential to drive an early exsolution geodynamo. *Geophys. Res. Lett.* **45**, 13,240-13,248 (2018).
23. D. Huang, J. Badro, Fe-Ni ideality during core formation on Earth. *Am. Mineral.* **103**, 1701–1710 (2018).

24. C. Cartier *et al*., Evidence for Nb 2+ and Ta 3+ in silicate melts under highly reducing conditions: A XANES study. *Am. Mineral.* **100**, 2152–2158 (2015).
25. B. Mysen, The structure of silicate melts. *Annu. Rev. Earth Planet. Sci.* **11**, 75–97 (1983).
26. D. Jana, D. Walker, The influence of sulfur on partitioning of siderophile elements. *Geochim. Cosmochim. Acta* **61**, 5255–5277 (1997).
27. D. Jana, D. Walker, The impact of carbon on element distribution during core formation. *Geochim. Cosmochim. Acta* **61**, 2759–2763 (1997).
28. J. Tuff, B. J. Wood, J. Wade, The effect of Si on metal-silicate partitioning of siderophile elements and implications for the conditions of core formation. *Geochim. Cosmochim. Acta* **75**, 673–690 (2011).
29. B. J. Wood, E. S. Kiseeva, F. J. Mirolo, Accretion and core formation: The effects of sulfur on metal-silicate partition coefficients. *Geochim. Cosmochim. Acta* **145**, 248–267 (2014).
30. Z. Ma, Thermodynamic description for concentrated metallic solutions using interaction parameters. *Metall. Mater. Trans., B, Process Metall. Mater. Proc. Sci.* **32**, 87–103 (2001).
31. J. Wade, B. J. Wood, Core formation and the oxidation state of the Earth. *Earth Planet. Sci. Lett.* **236**, 78–95 (2005).
32. R. B. Georg, A. Shahar, The accretion and differentiation of Earth under oxidizing conditions. *Am. Mineral.* **100**, 2739–2748 (2015).
33. B. J. Wood, D. J. Smythe, T. Harrison, The condensation temperatures of the elements: A reappraisal. *Am. Mineral.* **104**, 844–856 (2019).
34. I. H. Campbell, H. S. O'Neill, Evidence against a chondritic Earth. *Nature* **483**, 553–558 (2012).
35. W. F. Mcdonough, S. Sun, The composition of the earth. *Chem. Geol.* **2541**, 223–253 (1995).
36. M. J. Walter, Y. Thibault, Partitioning of tungsten and molybdenum between metallic liquid and silicate melt. *Science* **1345**, 13–16 (1995).
37. D. Andrault *et al*., Solidus and liquidus profiles of chondritic mantle: Implication for melting of the Earth across its history. *Earth Planet. Sci. Lett.* **304**, 251–259 (2011).
38. G. Fiquet *et al*., Melting of peridotite to 140 gigapascals. *Science* **329**, 1516–1518 (2010).
39. L. R. Benedetti, P. Loubeyre, Temperature gradients, wavelength-dependent emissivity, and accuracy of high and very-high temperatures measured in the laser-heated diamond cell. *High Press. Res.* **24**, 423–445 (2004).
40. Y. Akahama, H. Kawamura, High-pressure Raman spectroscopy of diamond anvils to 250 GPa: Method for pressure determination in the multimegabar pressure range. *J. Appl. Phys.* **96**, 3748–3751 (2004).
41. Japan Society for the Promotion of Science and Nineteenth Committee on Steelmaking, *Steelmaking Data Sourcebook*, (Gordon and Breach Science Publishers, New York, 1988).

PNAS
www.pnas.org

Supplementary Information for

The niobium and tantalum concentration in the mantle constrains the composition of Earth's primordial magma ocean

Dongyang Huang[a,1], James Badro[a], Julien Siebert[a,b]

[a]Institut de Physique du Globe de Paris, Sorbonne Paris Cité, 75005 Paris, France; [b]Institut Universitaire de France, France

[1]To whom correspondence should be addressed.

Email: huang@ipgp.fr

This PDF file includes:

Supplementary text
Figure S1-S5
Tables S1 to S3
Legend for Dataset S1-S2
SI References

Other supplementary materials for this manuscript include the following:

Dataset S1
Dataset S2

Supplementary Information Text

Synthesis of starting materials

Silicate glass: High purity oxides (MgO, Al_2O_3, and SiO_2, with or without NiO) and carbonate ($CaCO_3$) doped with Nb, Ta (sometimes with Cr and V, added as ICP standard solutions) were ground in ethanol in an agate mortar and then decarbonated, compressed and transformed into a glass in an Argon flux using aerodynamic levitation furnace coupled with 120 W CO_2 laser.

Starting metal: The piston-cylinder experiment was performed at 2 GPa and 1800 °C in a MgO capsule with graphite furnace and $BaCO_3$ cell assembly. Natural MORB was ground and mixed with high purity oxides (NiO and Cr_2O_3) and ICP vanadium standard solutions and fired at 950 °C overnight and then mixed and equilibrated with silicon-bearing iron alloy under high P-T for 2 minutes. Chemical homogeneity for both silicate and metal was confirmed by EPMA analysis, as reported in Table S2.

Sample recovery and analyses

After quench and decompression, thin sections were extracted from the center of the laser-heated area using a Ga^+ focused ion beam (FIB) instrument equipped with a field emission gun (Zeiss Auriga 40) at IPGP. Both secondary and backscattered electron images were used to monitor the sectioning. To avoid any possible contamination from adjacent phases in EDX or EPMA analysis, samples were sectioned down to 3-4 µm thick with the same geometry on both sides. Thin sections were removed from the center of the laser-heated spot by an in situ micromanipulator, and then welded to TEM copper grids with carbon deposit for further polishing and metalized for later analysis. An image of the recovered DAC sample is shown as an example in Fig. 1.

Chemical analysis of both metal and silicate phases was performed using electron probe micro-analysis (EPMA) on a Cameca SX-five at Camparis. An accelerating voltage of 15 kV and a beam current of 40 nA were used in all cases. Peak and background counting times were 15 s for major elements (Mg, Al, Ca, Fe and Si) in the silicate melts and for Fe in the quenched metals, and 60 s for minor and trace elements (Ta, Nb, Ni, V, and Cr) in both silicate and metallic phases, including Si, O, Mg, and Al in the metal, given that the detection limits were 100-400 ppm for most elements, except for Ni, Cr, V, Nb and Ta, who were more likely to be detected above 400 ppm. Diopside (Ca and Mg), orthoclase (Al and Si), hematite (Fe and O), vanadinite (V), NiO for Ni, Cr_2O_3 (Cr), and pure Nb, Ta metals were employed as internal standards. Nb was analyzed using $L_{\alpha 1}$ line, Ta using M_{α} line whereas all other elements using $K_{\alpha 1}$ line. Special care was taken to avoid analytical contamination: when the size of quenched silicate or metallic melts was comparable to the interaction volume, small beam (< 1 µm) was used and the analyzed spots were chosen far enough from the metal-silicate interface to avoid any secondary fluorescence from adjacent phases. For each phase in an individual run, 5-7 spots/windows were measured by microprobe.

Quantitative analysis was also conducted using energy dispersive X-ray (EDX) spectroscopy on FEG-FIB at IPGP. Excellent agreement was achieved for both techniques except for run X16, which has a strong fluorescence effect from surrounding silicate when analyzing the metal with EPMA, due to the large beam relative to the metal. For this reason, we opt for EDX analysis only for run X16. Accuracy of the measurements is expected to be 1 % based on the analytical calibrants.

Oxidation states of Nb and Ta in silicate melt

It has been shown by XANES measurements that Nb and Ta are pentavalent (5+) in silicate melts in moderately reducing conditions (fO_2 higher than IW-4) (1, 2). With our experiments being performed in this range of fO_2 (from IW-1 to -2, Table S1), it is reasonable to assume that Nb and Ta should remain in the 5+.

However, the valence state of a cation in silicate melt can also be determined by plotting the partition coefficient logD as a function of fO_2, at a given P and T, which must show a slope of -n/4 where n is the cation's valence. We plotted logD vs. log fO_2 in Fig. S1. We used all available experimental data (published and our data) at an fO_2 higher than IW-4. We found that the valence of Nb is 4.6 +/- 0.3 and that of Ta is 4.9 +/- 0.3. Rounded to the nearest integer, this confirms that both those elements remain pentavalent up to 94 GPa and 4500 K.

The oxygen fugacity relative to the iron-wüstite (IW) buffer is:

$$log\ fO_2 = 2\ log\left(\frac{a_{FeO}^{sil}}{a_{Fe}^{met}}\right), \qquad (S1)$$

where a_{FeO}^{sil} and a_{Fe}^{met} are the activities of FeO and Fe in the silicate and metal. This allows to express the partition coefficient explicitly as a function of fO_2 by rearranging Eq. 2 (the equilibrium constant) as:

$$log\ D\ (M) = -\frac{n}{4} log\ fO_2 + a + \frac{b}{T} + \frac{c \cdot P}{T} + d \cdot \left(\frac{nbo}{t} - 2.7\right) - log\ \gamma_M^{metal} \qquad (S2)$$

This can be rewritten as:

$$logD^*(M) = log\ D\ (M) - \frac{b}{T} - \frac{c \cdot P}{T} - d \cdot \left(\frac{nbo}{t} - 2.7\right) + log\ \gamma_M^{metal} = a - \frac{n}{4} log\ fO_2 \qquad (S3)$$

where D* is basically the partition coefficient corrected for P, T, and activity dependence. The calculations of Eq. S3 were based on measurements (Dataset S1) and parameters tabulated in Table 1. The valence state can then be obtained from the slope of logD* vs. log fO_2 in Fig. S1. Ordinary least square (OLS) regression yields n = 4.6 +/- 0.3, R^2 = 0.83 for Nb; and n = 4.9 +/- 0.3, R^2 = 0.83 for Ta. Rounded to the nearest integer, and fully consistent with all previous data, we used 5+ for both cations. Note that the valence fit is identical within uncertainties ***with*** and ***without*** our DAC data, as is shown here:

Valence Fit	Nb	Ta
Literature + This work	4.6(3)+	4.9(3)+
Literature data	4.7(3)+	5.0(3)+

Activity model for metal

To model the interactions in the metal and to correct the effects of the alloy composition on partitioning, we used the thermodynamically consistent interaction parameter (ε) approach proposed by (3), to calculate the activity coefficients of γ_{Fe} and γ_i, which has become standard practice (4–8). Following the method, the activity coefficients of the solvent (Fe) and N-1 solutes (i) for N components metallic solutions can be expressed as:

$$\ln\gamma_{Fe} = \sum_{i=1}^{N-1} \varepsilon_i^i (X_i + \ln(1-X_i)) - \sum_{j=1}^{N-2}\sum_{k=j+1}^{N-1} \varepsilon_j^k X_j X_k \left(1 + \frac{\ln(1-X_j)}{X_j} + \frac{\ln(1-X_k)}{X_k}\right)$$
$$+ \sum_{i=1}^{N-1}\sum_{\substack{k=1 \\ (k\neq i)}}^{N-1} \varepsilon_i^k X_i X_k \left(1 + \frac{\ln(1-X_k)}{X_k} - \frac{1}{1-X_i}\right) + \frac{1}{2}\sum_{j=1}^{N-2}\sum_{k=j+1}^{N-1} \varepsilon_j^k X_j^2 X_k^2 \left(\frac{1}{1-X_j} + \frac{1}{1-X_k} - 1\right) \quad (S4)$$
$$- \sum_{i=1}^{N-1}\sum_{\substack{k=1 \\ (k\neq i)}}^{N-1} \varepsilon_i^k X_i^2 X_k^2 \left(\frac{1}{1-X_i} + \frac{1}{1-X_k} + \frac{X_i}{2(1-X_i)^2} - 1\right)$$

and

$$\ln\gamma_i = \ln\gamma_{Fe} + \ln\gamma_i^0 - \varepsilon_i^i \ln(1-X_i) - \sum_{j=1(j\neq i)}^{N-1} \varepsilon_i^j X_j \left(1 + \frac{\ln(1-X_j)}{X_j} - \frac{1}{1-X_i}\right)$$
$$+ \sum_{j=1(j\neq i)}^{N-1} \varepsilon_i^j X_j^2 X_i \left(\frac{1}{1-X_i} + \frac{1}{1-X_j} + \frac{X_i}{2(1-X_i)^2} - 1\right) \quad (S5)$$

where γ_i^0 is the activity coefficient of solute i in liquid iron at infinite dilution, ε_i^j the interaction parameter of element j on element i and X_i the mole fraction of element i in the metal. Interactions between minor/trace metals are not considered, since their influence on each other are supposed to be negligible due to the low abundances. We fitted ε_i^j between light-element species (Si, O, C, and S) and minor/trace metals, including their self-interaction parameters ε_i^i, at the reference temperature 1873 K (T^0) and reported them in Table 1, together with γ_i^0 taken from *Steelmaking Data Sourcebook* (Japan Society for the Promotion of Science and the Nineteenth Committee on Steelmaking, 1988). ε_i^j and γ_i^0 were then extrapolated to run temperatures according to:

$$\ln\gamma_i^0(T) = \frac{T^0}{T}\ln\gamma_i^0(T^0) \quad (S6)$$

$$\varepsilon_i^j(T) = \frac{T^0}{T}\varepsilon_i^j(T^0) \quad (S7)$$

Following Eq. 2, the equilibrium constant K was calculated for data from literature and this study and plotted in Fig. 2.

Calculations of *nbo/t*

Following (9), *nbo* is calculated by 2*O – 4*t, where *O* is the number of oxygen atoms and *t* is the number of tetrahedral cations (including Al^{3+}, Si^{4+}, Ti^{4+}, P^{5+} and Fe^{3+}). Aluminum needs charge balance in order to be tetrahedrally coordinated, the requirement for Al^{3+} charge-compensation ($Al^{3+} < Na^{+}+K^{+}+0.5(Ca^{2+}+Mg^{2+})$) is met for all silicate composition in this study. At low oxygen fugacity conditions of our experiments almost all Fe is expected in 2+ oxidation state, therefore Fe is not considered as a possible network-forming cation occurring in tetrahedral coordination. This gives *nbo/t* values of 2 for an end member Diopside composition and 2.75 for a peridotite KLB1 composition. The calculated *nbo/t* are reported in Dataset S1.

Dependence on silicate melt composition

It has been shown that silicate melt composition, particularly the degree of polymerization which is conveniently parameterized as a function of *nbo/t*, can significantly affect the partitioning behavior between metal and silicate (10–13), especially for high valence state cations Nb and Ta. Due to the fact that the coordination environment in silicate changes from tetrahedra to octahedra at upper mantle conditions (10 to 20 GPa), the *nbo/t* calculation is no longer applicable to our higher P data (> 40 GPa),

we only calculated and fitted the *nbo/t* values for previous data less than 25 GPa and kept our *nbo/t* constant at the pyrolitic value of 2.7. The equilibrium constant K in log units is plotted as a function of *nbo/t* in Fig. S2.

The log K scatters in a range of about 2 log units even with the identical *nbo/t* values, and there is no resolvable compositional dependence regarding the degree of polymerization of silicate melt, as illustrated by the log K of Nb in Fig. S2 (open circles). This can be explained by the multiple effects of P, T and metal composition, which are not shown here and are discussed in the main manuscript. The degree of the scattering lessens and the compositional effect starts to emerge when correcting for the effects of P and T by simply subtracting the a and b terms, as can be seen from the solid circles plotted using the same dataset. In agreement with previous observations (14), Nb become more lithophile in more depolymerized melt (higher *nbo/t*), whereas pentavalent Ta is only observed to a much lesser extent. The reason, since they are not considered tetrahedral cations, may be that highly charged Nb and Ta cations require more non-bridging oxygen atoms in order to be stably incorporated in the silicate network.

Bulk *D* between Earth's core and mantle for Nb, Ni and Co

The targets (observables) to match in core formation models are the bulk partition coefficient (*D*) between Earth's core and mantle for Nb, Ni and Co, and the subchondritic Nb/Ta ratio observed in the BSE (15). The calculation of these bulk *D*s is described in detail here. Ta, on the other hand, has no target of *D* to match, in light of the well-established assumption that it is purely lithophile, which is consistent with our calculated bulk *D* for Ta close to zero (see Fig. 3 and Fig. S4).

Firstly, the concentration of an interested element in the bulk silicate Earth (x_{BSE}) is compiled from ref. (16) and ref. (17). Second, late veneer contribution is corrected assuming that the accreting materials after core formation are chondritic in its composition:

$$x_{BSE}^{LV} = \frac{f \cdot x_{BSE} - f_{LV} \cdot x_{CI}}{f - f_{LV}} \quad (S8)$$

where x_{BSE}^{LV} is the concentration in the BSE after core formation and before late veneer, f the mass fraction of the mantle in Earth which equals 0.68M_E, f_{LV} the mass fraction of the chondritic material delivered during later veneer which is estimated to be 0.005M_E, and x_{CI} the concentration in CI chondrites which is also taken from ref. (16) and ref. (17). Third, the bulk D between core and mantle after core formation can be calculated by:

$$D = \frac{(R \cdot x_{CI} - x_{BSE}^{LV}) \cdot \frac{f}{1-f}}{x_{BSE}^{LV}} \quad (S9)$$

where the numerator is the concentration of the interested element in the core. R is the average ratio of refractory lithophile elements (RLEs) concentrations or the ratio of magnesium (Mg) concentrations, between BSE and CI chondrites: for refractory elements, R equals 2.87; for elements (Ni, Co, Cr) having similar 50% condensation temperatures as Mg (T_{50} = ~1340 K) in the solar nebular, R equals 2.35. *R* is calculated from refs (17–19). $R \cdot x_{CI}$ therefore represents the content of the interested element in the BSE without any loss into the core, $(R \cdot x_{CI} - x_{BSE}^{LV}) \cdot f$ is the mass of the element sequestrated in the core, and $(R \cdot x_{CI} - x_{BSE}^{LV}) \cdot \frac{f}{1-f}$ the concentration of the interested element in the core. As can be seen in Eq. S8, the underlying assumption for this calculation is that Earth's building blocks are CI-like materials. Given $x_{BSE} = 0.595\, ppm$ and $x_{CI} = 0.283\, ppm$ with 20% and 10% uncertainties respectively, the calculated bulk $D_{\text{core-mantle}}$ for Nb equals 0.8 +/- 0.5. The calculated bulk $D_{\text{core-mantle}}$ is used as the targets in our core formation model and is listed in Dataset S2. The calculations are also performed for other carbonaceous chondrites and are reported in Dataset S2.

Effect of disequilibrium on core formation models

Our results do not address disequilibrium between the core and mantle during large impacts (e.g., Moon-forming giant impact), because such models have to assume a composition for the impactor (20, 21), which is not well constrained. Although our model does not require disequilibrium, if we assume the negative correlation between the degree of disequilibrium and Nb/Ta ratio in the BSE as in ref. (22), during late stages such giant impact would equally lower the Nb/Ta ratio in Fig. 3b, making the most reduced scenarios even less favorable, while oxidized still feasible.

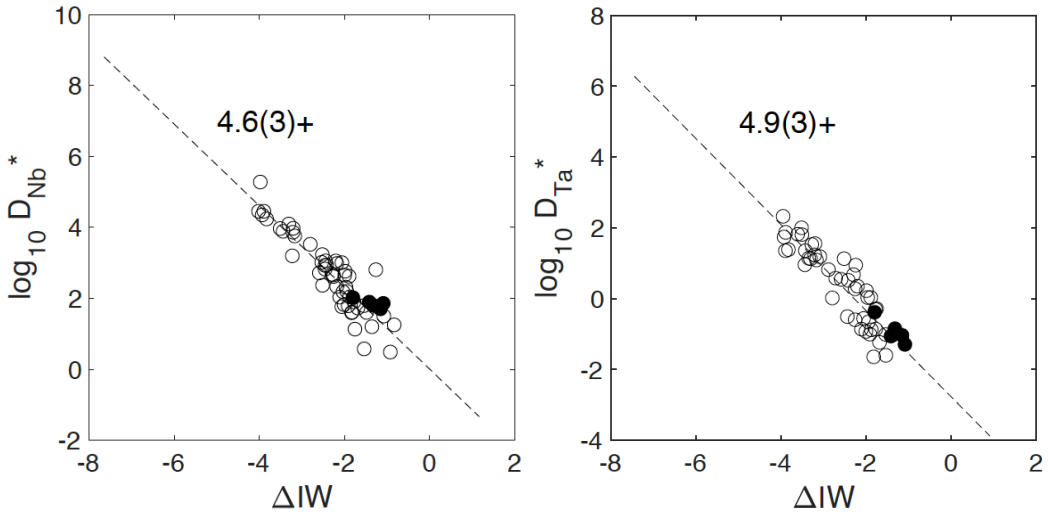

Fig. S1. Partition coefficients of Nb and Ta as a function of oxygen fugacity relative to the iron-wüstite buffer (ΔIW). Log D* denotes corrected values using Eq. S3. The regressions were performed with data collected at fO_2 above IW-4 from the literature (open circles) and our data (solid circles). The fitted oxidation states are close to 5+: 4.6+ and 4.9+ for Nb and Ta, respectively.

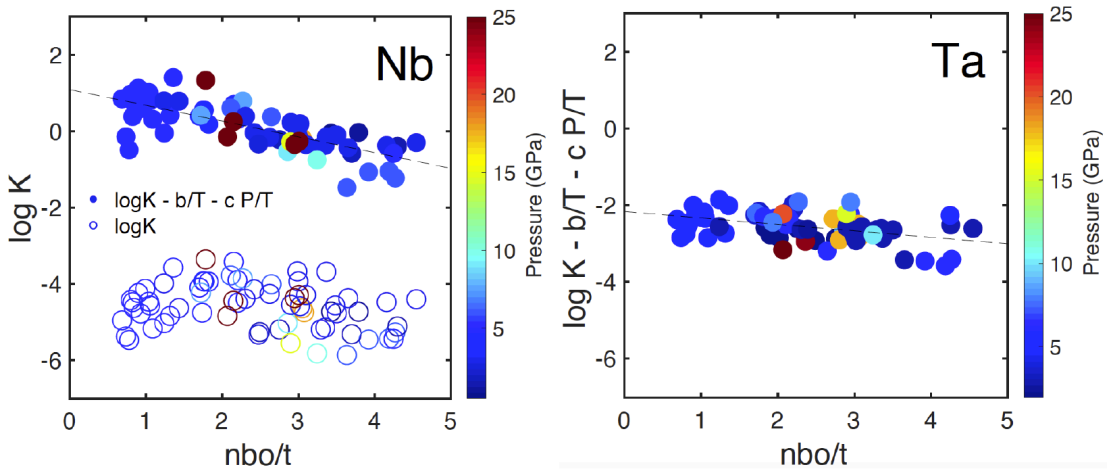

Fig. S2. Equilibrium constants (log K) for experiments conducted under 25 GPa as a function of *nbo/t* for Nb and Ta. No resolvable trend can be seen for log K of Nb (open circles), due to the combined effect of pressure and temperature. When P and T effects (*c* and *b* terms in Eq. 3) are corrected for, i.e., log K -*b*/T -*c* P/T (solid circles), Nb is found weakly dependent on the silicate melt composition, while no significant dependence is observed for Ta, consistent with ref. (14).

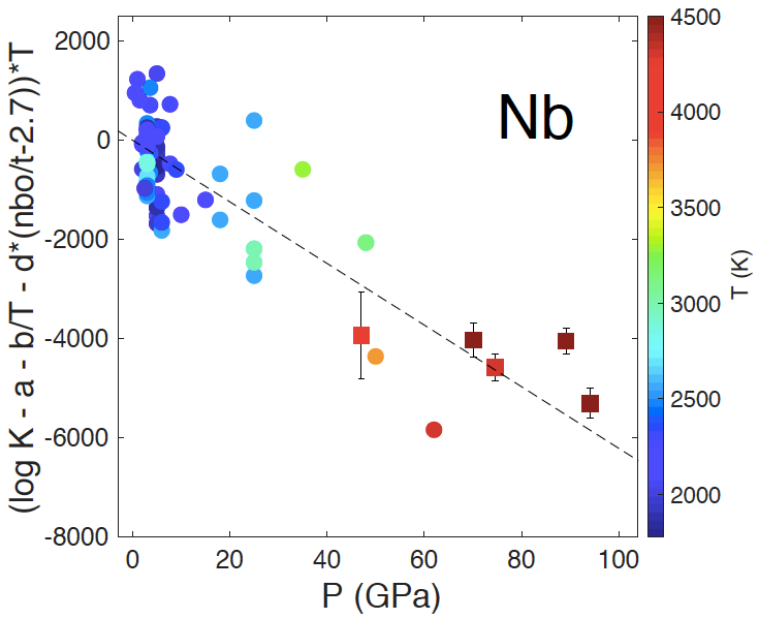

Fig. S3. Equilibrium constants (log K) for Nb as a function of pressure by correction to zero temperature and pyrolitic composition. Temperature is reported in symbol color. The dataset are the same as in Fig. 2 from (4, 7, 14, 23–27) (circles) and this study (squares). The corrected values of log K decrease with increasing pressure, i.e. Nb becomes less siderophile with pressure.

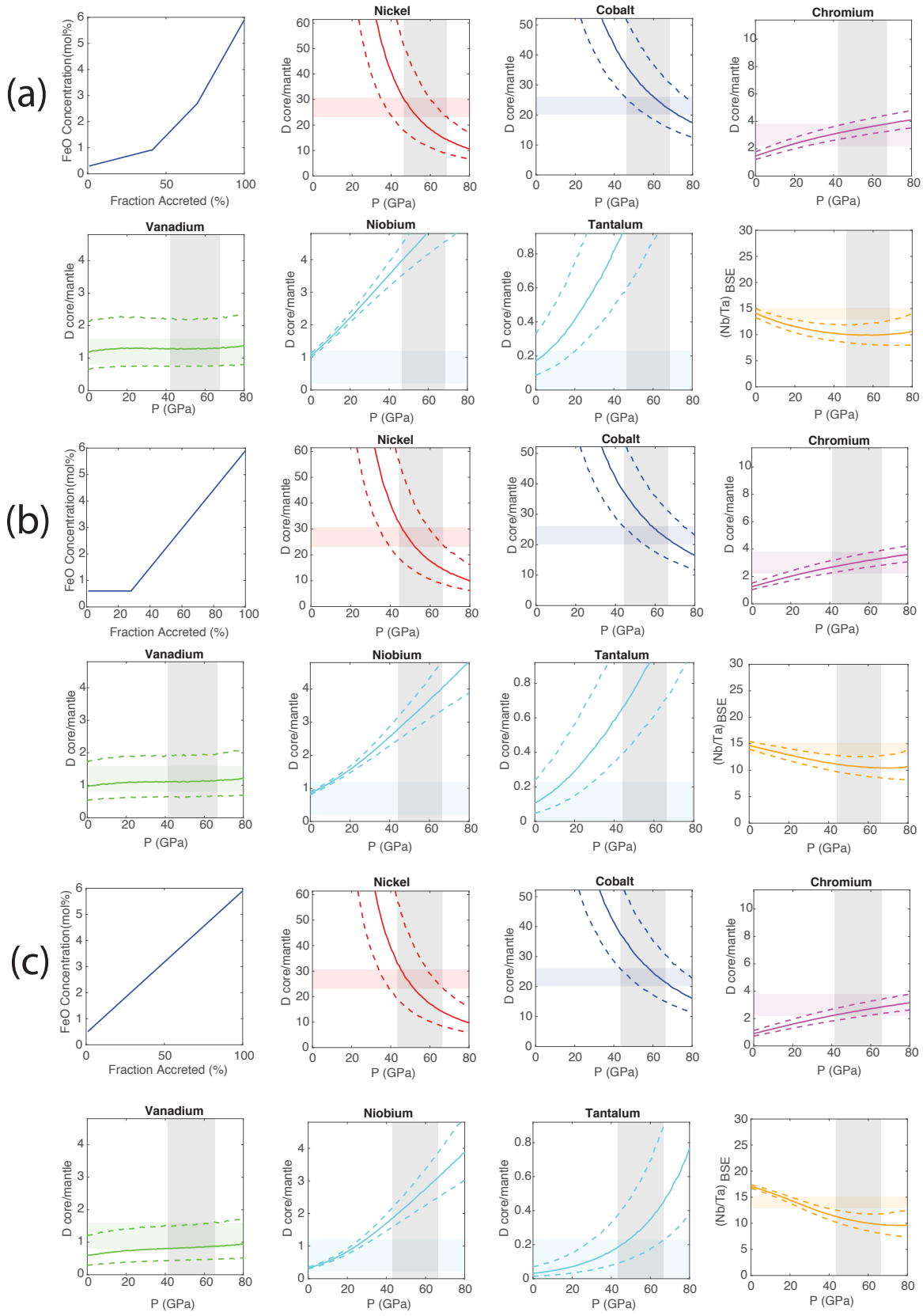
(a)
(b)
(c)
FeO Concentration(mol%)
Fraction Accreted (%)
Nickel
Cobalt
Chromium
Vanadium
Niobium
Tantalum
D core/mantle
(Nb/Ta) BSE
P (GPa)

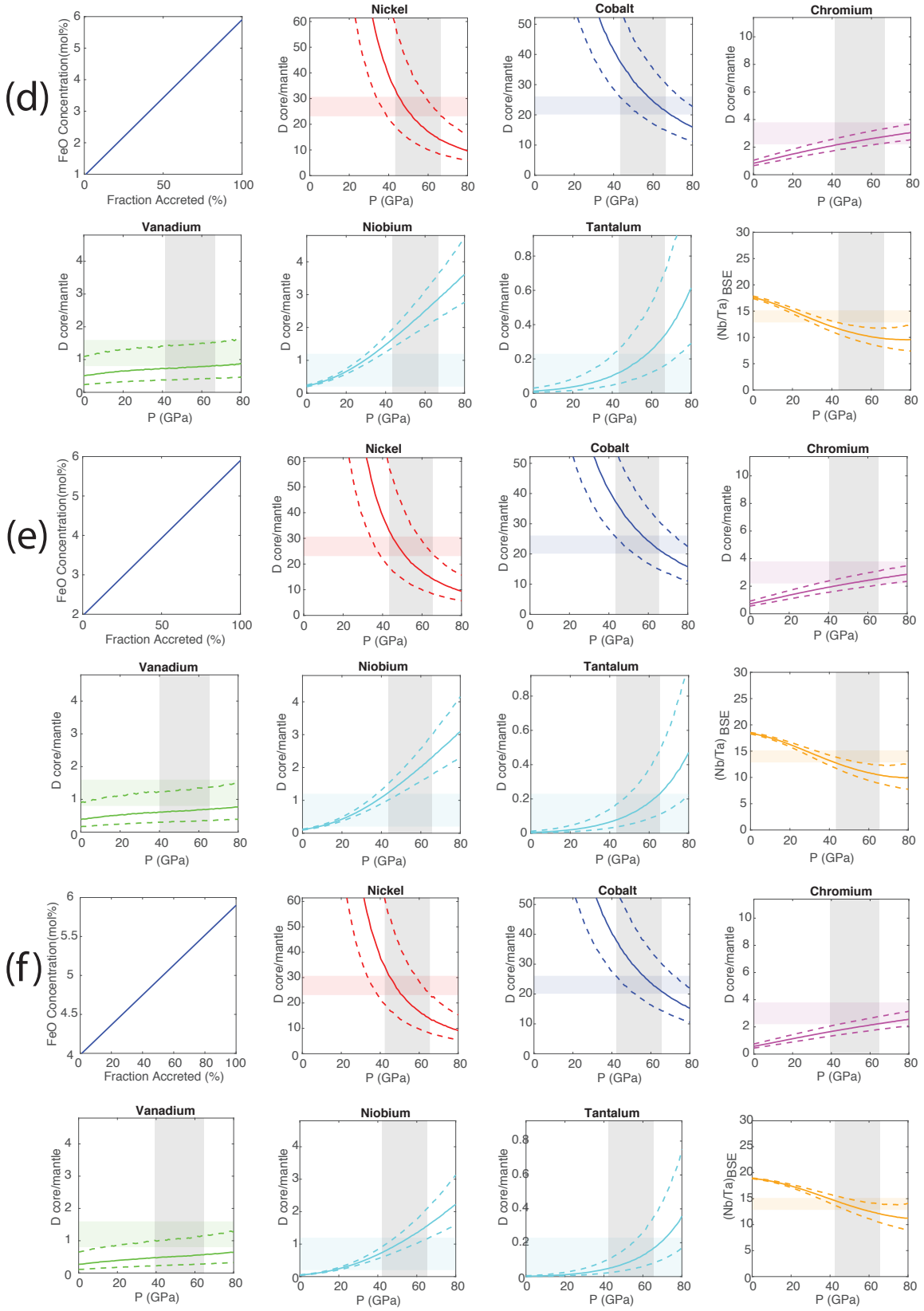
(d)
FeO Concentration(mol%)
Fraction Accreted (%)
Nickel
Cobalt
Chromium
D core/mantle
P (GPa)
Vanadium
Niobium
Tantalum
(Nb/Ta) BSE
(e)
(f)

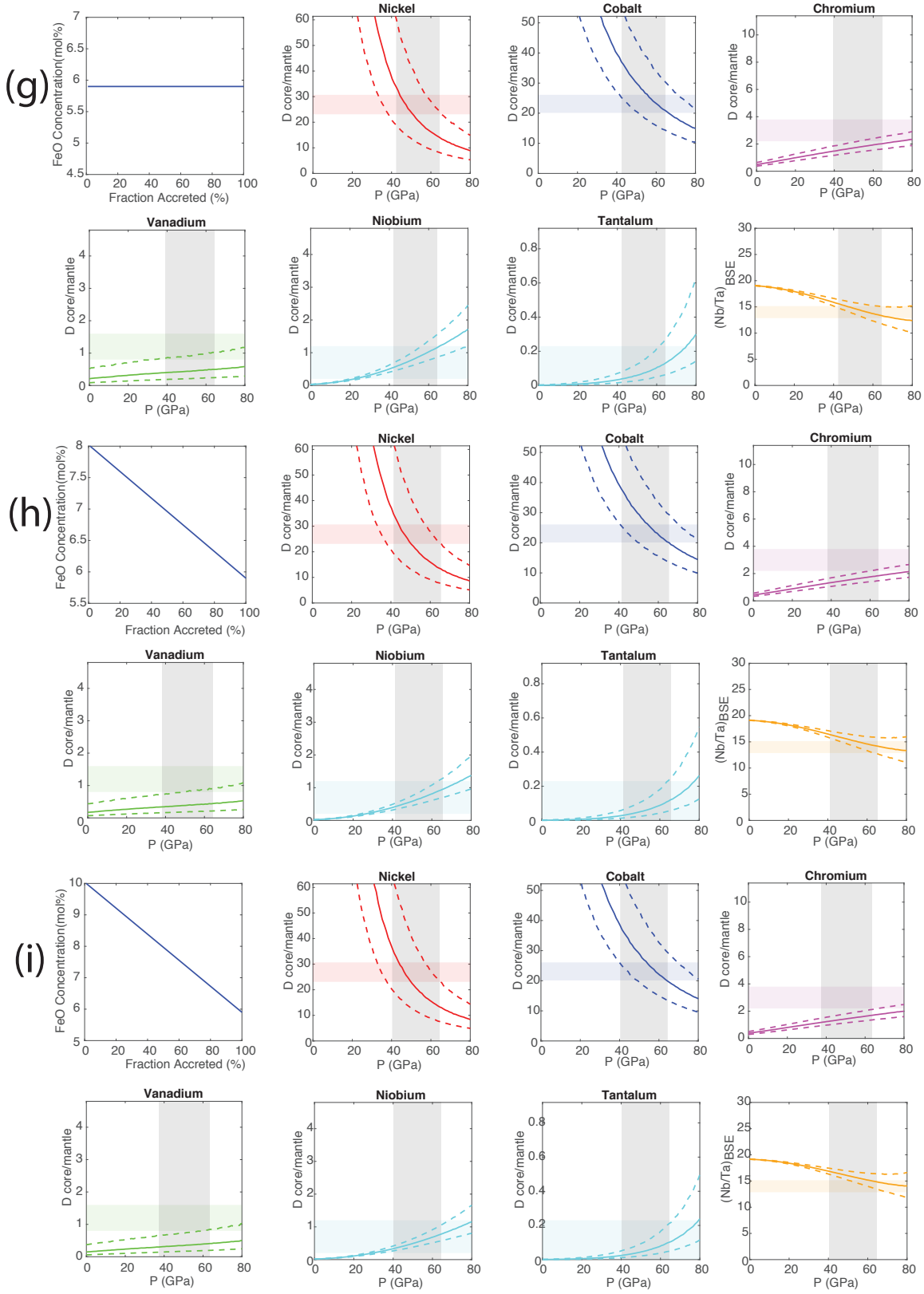
(g)
(h)
(i)
FeO Concentration(mol%)
Fraction Accreted (%)
Nickel
Cobalt
Chromium
Vanadium
Niobium
Tantalum
D core/mantle
P (GPa)
(Nb/Ta)BSE

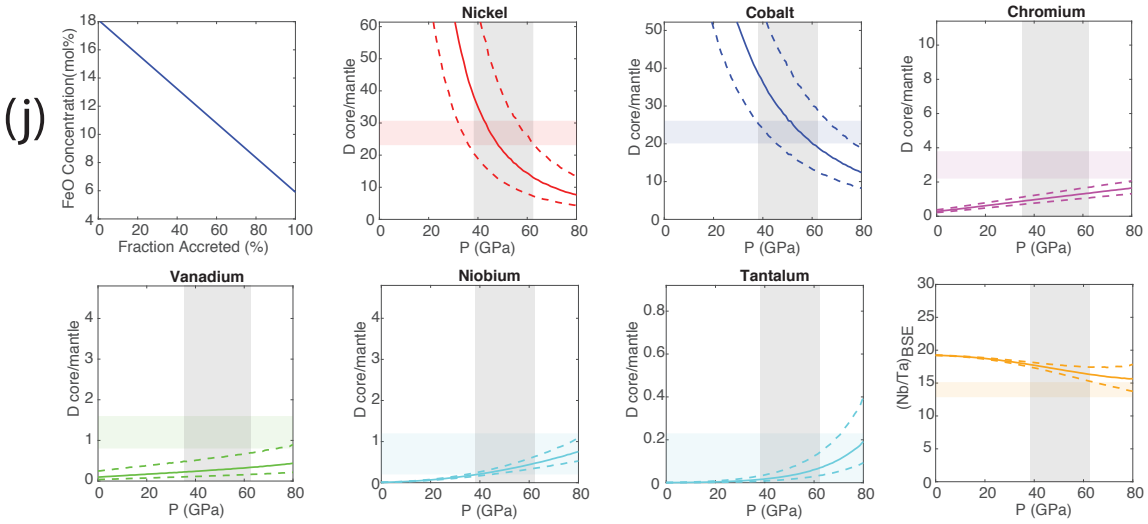

Fig. S4. Core-mantle partition coefficients of Ni, Co, Cr, V, Nb and Ta, and Nb/Ta ratio in the bulk silicate Earth (BSE) as a function of final magma ocean pressure under a range of fO_2 paths (a-j), corresponding to those of Fig. 3a. The horizontal bars correspond to the targets (present-day subchondritic Nb/Ta ratio in BSE or bulk D between core and mantle); whereas the vertical shaded area is the pressure range allowed by the observables of Ni and Co partitioning. Simultaneous match of the observables (intersections of horizontal and vertical bars) cannot be reproduced under highly reducing (a-d) nor oxidizing (h) redox conditions. The initial FeO content of Earth's magma ocean is therefore constrained to between 2 and 18 mol% (e-i).

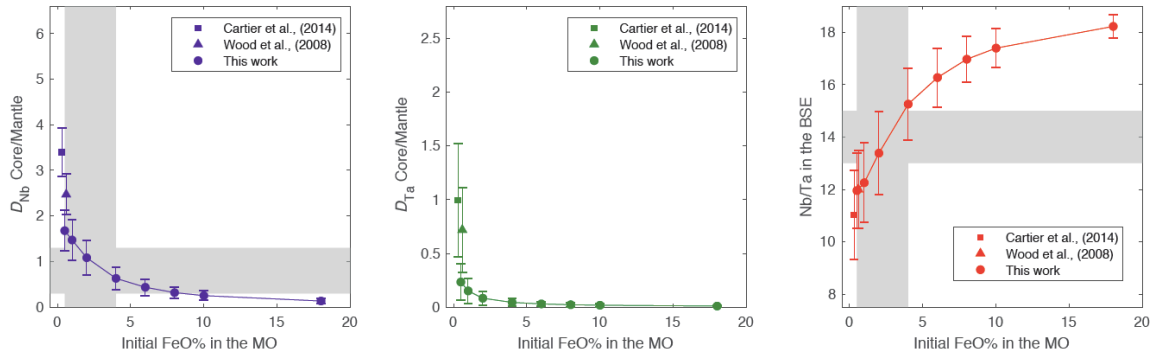

Fig. S5. Core-mantle partition coefficients of Nb (blue) and Ta (green) and Nb/Ta ratio (red) in the bulk silicate Earth (BSE) at the end of Earth's accretion, as a function of initial FeO content (in mol%) in the magma ocean (MO), ***without*** the effect of oxygen interaction. In order to test the model with low-pressure data, all the input parameters are kept the same as in Fig. 3, except that the oxygen content in the core (or ε_i^O) is set to zero (i.e., no interaction with oxygen). Without interacting with oxygen, the redox condition required to reproduce D_{Nb} and Nb/Ta in the BSE is limited to the canonical reduced conditions as shown by the vertical shaded area, which is advocated by partitioning experiments performed at relatively low pressures up to ~25 GPa (4, 23, 27, 28).

Table S1. Runs summary.

Exp. No.	X17-1	X6-1	X17-2	X9-1	X16
Pressure (GPa)	47±5	70±7	75±7	89±9	94±9
Temperature (K)	4100±200	4500±250	4300±220	4500±250	4500±250
Starting Silicate [a]	Pyrolite + Nb Ta	Pyrolite + Nb Ta	Pyrolite + Nb Ta Ni Cr V	Pyrolite + Nb Ta Ni Cr V	Pyrolite + Nb Ta Ni Cr V
Starting Metal	Fe-Si alloy (9wt% Si)	Fe-Ni alloy (by piston-cylinder)	Fe-Si alloy (9wt% Si)	Fe-Si alloy (9wt% Si)	Fe-Si alloy (9wt% Si)
fO_2 (ΔIW) [b]	-1.9	-1.5	-1.4	-1.2	-1.2

Notes:

a: All pyrolite are FeO-free.

b: Oxygen fugacity relative to the iron-wustite buffer is approximated as $fO_2(\Delta IW) = \log_{10}(xFe/xFeO)$, assuming ideal mixing.

Table S2. Starting material compositions measured by EPMA (σ corresponding to 1 standard deviations of multiple measurements).

	wt%	**σ**
Fe-Ni alloy		
O	0.22	0.02
Si	2.25	0.01
V	0.83	0.01
Cr	0.91	0.01
Fe	91.49	0.19
Ni	3.75	0.03
Total	99.45	0.19
Pyrolite + Nb Ta		
MgO	39.24	0.10
Al2O3	4.34	0.01
SiO2	50.63	0.03
CaO	2.49	0.02
Nb2O5	1.65	0.03
Ta2O5	1.26	0.06
Total	99.63	0.12
Pyrolite + Nb Ta Ni Cr V		
MgO	36.08	0.07
Al2O3	4.17	0.01
SiO2	49.38	0.02
CaO	2.32	0.01
V2O3	1.33	0.02
Cr2O3	0.32	0.01
NiO	3.45	0.02
Nb2O5	1.53	0.03
Ta2O5	1.22	0.05
Total	99.81	0.1

Table S3. EPMA results for metal and silicate (σ corresponding to 1 standard deviations of multiple measurements).

Metal

Exp. No.		N	O	Mg	Al	Si	V	Cr	Fe	Ni	Nb	Ta	Total
X16[1]	wt%	3	6.55	0.94	0.18	3.06	1.97	3.88	29.26	48.65	2.24	3.02	100.00
	σ		0.30	0.15	0.05	0.23	0.13	0.07	0.19	0.90	0.11	0.43	-
X9-1	wt%	6	5.52	0.64	0.14	4.09	2.29	4.05	31.96	38.86	3.00	0.82	91.26
	σ		0.28	0.27	0.05	0.10	0.05	0.06	0.23	0.59	0.06	0.08	0.37
X6-1	wt%	5	5.53	0.42	0.11	9.01	0.25	0.46	75.31	3.52	1.58	0.80	97.01
	σ		0.19	0.03	0.01	0.07	0.02	0.02	0.10	0.03	0.06	0.08	0.22
X17-1	wt%	5	3.52	0.46	0.06	12.28	0.00	0.00	78.43	0.00	2.40	0.60	97.80
	σ		0.37	0.33	0.01	0.34	0.00	0.00	0.62	0.00	0.05	0.12	0.64
X17-2	wt%	5	5.07	0.45	0.09	5.08	1.71	2.95	50.76	25.36	2.23	0.69	94.32
	σ		0.27	0.32	0.02	0.18	0.05	0.03	0.20	0.10	0.07	0.11	0.42

Silicate

Exp. No.		N	MgO	SiO2	CaO	FeO	NiO	Al2O3	CrO	V2O3	Nb2O5	Ta2O5	Total
X16[1]	wt%	6	26.75	28.34	2.30	8.19	9.48	5.87	3.62	4.36	5.48	5.60	100.00
	σ		0.59	0.63	0.16	0.46	0.63	0.17	0.11	0.10	0.15	0.40	-
X9-1	wt%	7	24.03	26.09	2.36	9.78	7.95	5.20	4.21	4.53	5.72	3.50	93.37
	σ		0.66	0.54	0.06	0.39	0.42	0.05	0.17	0.18	0.30	0.17	0.31
X6-1	wt%	6	32.19	35.81	2.77	18.47	0.64	6.11	0.38	0.44	1.94	1.54	100.28
	σ		1.95	1.30	0.13	1.10	0.04	0.19	0.03	0.03	0.13	0.18	2.04
X17-1	wt%	6	33.21	45.75	2.66	11.40	0.00	3.97	0.00	0.00	2.60	1.48	101.09
	σ		1.46	0.57	0.15	2.20	0.03	0.17	0.00	0.00	0.18	0.12	1.20
X17-2	wt%	5	31.31	29.83	2.64	11.46	3.47	6.19	2.77	3.32	4.03	2.91	97.93
	σ		0.53	0.43	0.05	0.56	0.33	0.15	0.03	0.06	0.20	0.13	0.54

Notes: [1]Measured by energy dispersive X-ray spectroscopy (EDX), data normalized to 100%.

Dataset S1 (separate file). Nb and Ta data employed in our thermodynamic model. Dataset includes element concentrations in Fe-rich alloys and silicate melts (in mole fraction), and *nbo/t* values.

Dataset S2 (separate file). Bulk partition coefficients between Earth's core and mantle for Ni, Co and Nb, calculated from element concentrations in the bulk silicate Earth and carbonaceous chondrites.

References

1. A. D. Burnham, A. J. Berry, B. J. Wood, G. Cibin, The oxidation states of niobium and tantalum in mantle melts. *Chem. Geol.* **330**–**331**, 228–232 (2012).
2. C. Cartier, *et al.*, Evidence for Nb 2+ and Ta 3+ in silicate melts under highly reducing conditions: A XANES study. *Am. Mineral.* **100**, 2152–2158 (2015).
3. Z. Ma, Thermodynamic description for concentrated metallic solutions using interaction parameters. *Metall. Mater. Trans. B* **32**, 87–103 (2001).
4. J. Wade, B. J. Wood, Core formation and the oxidation state of the Earth. *Earth Planet. Sci. Lett.* **236**, 78–95 (2005).
5. A. Corgne, J. Siebert, J. Badro, Oxygen as a light element: A solution to single-stage core formation. *Earth Planet. Sci. Lett.* **288**, 108–114 (2009).
6. A. Ricolleau, Y. Fei, A. Corgne, J. Siebert, J. Badro, Oxygen and silicon contents of Earth's core from high pressure metal-silicate partitioning experiments. *Earth Planet. Sci. Lett.* **310**, 409–421 (2011).
7. J. Siebert, J. Badro, D. Antonangeli, F. J. Ryerson, Terrestrial Accretion Under Oxidizing Conditions. *Science (80-.).* **339**, 1194–1197 (2013).
8. R. A. Fischer, *et al.*, High pressure metal-silicate partitioning of Ni, Co, V, Cr, Si, and O. *Geochim. Cosmochim. Acta* **167**, 177–194 (2015).
9. B. Mysen, The Structure of silicate melts. *Annu. Rev. Earth Planet. Sci.* **11**, 75–97 (1983).
10. M. J. Walter, Y. Thibault, Partitioning of tungsten and molybdenum between metallic liquid and silicate melt. *Science (80-.).* **1345**, 13–16 (1995).
11. D. Jana, D. Walker, The influence of silicate melt composition on distribution of siderophile elements among metal and silicate liquids. *Earth Planet. Sci. Lett.* **150**, 463–472 (1997).
12. H. S. C. O'Neill, S. M. Eggins, The effect of melt composition on trace element partitioning: An experimental investigation of the activity coefficients of FeO, NiO, CoO, MoO2 and MoO3 in silicate melts. *Chem. Geol.* **186**, 151–181 (2002).
13. N. L. Chabot, C. B. Agee, Core formation in the Earth and Moon: New experimental constraints from V, Cr, and Mn. *Geochim. Cosmochim. Acta* **67**, 2077–2091 (2003).
14. J. Siebert, A. Corgne, F. J. Ryerson, Systematics of metal-silicate partitioning for many siderophile elements applied to Earth's core formation. *Geochim. Cosmochim. Acta* **75**, 1451–1489 (2011).
15. C. Münker, *et al.*, Evolution of planetary cores and the Earth-Moon system from Nb/Ta systematics. *Science (80-.).* **301**, 84–87 (2003).
16. W. F. Mcdonough, S. Sun, The composition of the earth. *Chem. Geol.* **2541**, 223–253 (1995).
17. H. Palme, H. O'Neill, *Cosmochemical Estimates of Mantle Composition*, 2nd Ed. (Elsevier Ltd., 2014).
18. J. A. Barrat, *et al.*, Geochemistry of CI chondrites: Major and trace elements, and Cu and Zn Isotopes. *Geochim. Cosmochim. Acta* **83**, 79–92 (2012).
19. K. Lodders, Solar System Abundances and Condensation Temperatures of the Elements. *Astrophys. J.* **591**, 1220–1247 (2003).
20. H. Piet, J. Badro, P. Gillet, Geochemical Constraints on the Size of the Moon-Forming Giant Impact. *Geophys. Res. Lett.* **44**, 11,770-11,777 (2017).
21. J. Wade, B. J. Wood, The oxidation state and mass of the Moon-forming impactor. *Earth Planet. Sci. Lett.* **442**, 186–193 (2016).
22. C. Munker, R. O. C. Fonseca, T. Schulz, Silicate Earth's missing niobium may have been sequestered into asteroidal cores. *Nat. Geosci.* **10**, 822–826 (2017).
23. C. Cartier, T. Hammouda, M. Boyet, M. A. Bouhifd, Redox control of the fractionation of niobium and tantalum during planetary accretion and core formation. *Nat. Geosci.* **7**, 573–576 (2014).
24. A. Corgne, S. Keshav, B. J. Wood, W. F. McDonough, Y. Fei, Metal-silicate partitioning and constraints on core composition and oxygen fugacity during Earth accretion. *Geochim. Cosmochim. Acta* **72**, 574–589 (2008).
25. U. Mann, D. J. Frost, D. C. Rubie, Evidence for high-pressure core-mantle differentiation from

the metal-silicate partitioning of lithophile and weakly-siderophile elements. *Geochim. Cosmochim. Acta* **73**, 7360–7386 (2009).
26. J. Siebert, J. Badro, D. Antonangeli, F. J. Ryerson, Metal-silicate partitioning of Ni and Co in a deep magma ocean. *Earth Planet. Sci. Lett.* **321**–**322**, 189–197 (2012).
27. J. Wade, B. J. Wood, The Earth's 'missing' niobium may be in the core. *Nature* **409**, 75–78 (2001).
28. B. J. Wood, J. Wade, M. R. Kilburn, Core formation and the oxidation state of the Earth: Additional constraints from Nb, V and Cr partitioning. *Geochim. Cosmochim. Acta* **72**, 1415–1426 (2008).